Aalborg
University

Student Report

Master's Thesis

# Assessment of Decellularized Scaffolds for Skeletal Muscle Engineering

Medicine with Industrial Specialization, biomedicine Group 9041
School of Medicine and Health, Aalborg University

**Department of Health Science and Technology**
Medicine with Industrial Specialization, Biomedicine

**Title:**
Assessment of Decellularized Scaffolds for Skeletal Muscle Engineering

**Semester:**
9-10

**Project period:**
1st of September 2021 – June 1st, 2022

**ECTS:**
60 points

**Project group:**
9041

**Supervisor:**
Cristian Pablo Pennisi

**Number of pages:**
41

**Participants:**

Hubert Krzylak
Hubert Krzylak

# Table of Contents

# Abstract

**Background:** Damage to muscles through various means can cause major disruption and a drastic decrease in muscle function. The current treatment options for these injuries are insufficient. Recent approaches consisting of transplantation of decellularized organ extracellular matrix (ECM) are also not without challenges. In vitro studies of human adipose derived stem cells (hASC) ECM have shown a promise for skeletal muscle regeneration with fiber alignment being a key factor for their differentiation. It is therefore of interest to investigate the effect on aligned hASC derived ECM's effect on skeletal muscle differentiation.

**Methods:** hASC were induced to deposit ECM on substrates consisting of either isotropic (aligned) or anisotropic (random) electrospun fibrous scaffolds. By qPCR, the transcriptional activity of ECM related genes collagen I, VI, fibronectin, and decorin was investigated. After decellularization, a colorimetric assay was used to determine the collagen content on the decellularized scaffolds. The expression of ECM proteins was examined by indirect immunofluorescent staining. C2C12 myoblasts were cultured on the decellularized scaffolds, and differentiation was assessed by colorimetric and immunofluorescent staining. On a pilot scale, human skeletal muscle myoblasts (hSkMM) were cultured and differentiated on the ECM scaffolds

**Results:** Alignment of the ECM with the underlying substrate was evident in the aligned scaffold. However, colorimetric assessment showed a marked decrease in collagen content in the aligned and random scaffolds. Indirect immunofluorescence showed a significant decrease in collagen I, VI, and fibronectin in both scaffold types. In addition, qPCR analysis showed a significant decrease in the expression of collagen I, VI, fibronectin and decorin at day 1, which persisted for collagen I and decorin at day 3. While a significant alignment of the myotubes was observed in the aligned scaffolds, the thickness, length, and abundance of myotubes decreased significantly in both scaffold types. Indirect immunofluorescence and Giemsa staining hSKMMs appear also to grow and differentiate favorably on ECM.

**Conclusions:** There is evidence that C2C12 differentiation is slightly better on ECM than without ECM. The alignment of both ECM and myotubes has been documented. However, it appears that the use of an ECM-coated aligned scaffold has no better effect on the differentiation of C2C12 myoblasts than ECM on a flat substrate. The promising results obtained with hSkMM differentiation may point to a new direction for future studies on the effect of hASC-derived ECM on skeletal muscle differentiation.

# 1 Introduction

## 1.1 Background

Damage to muscles exerted either through crushing forces, extreme cold, or toxins are called traumatic skeletal muscle injuries (TMI). These can cause major damage to the effected muscle area and thus causing a drastic decrease in muscle function (1). Some causes for TMI could be high energy trauma stemming from car-accidents, combat related injuries such as blast trauma, surgical interventions, or during various sports activities. In the US alone the cost of muscle injuries reaches 790 billion USD in annual healthcare spending (2). In sports specifically, up to 55% of all acquired injuries have damage on the myofiber level (3). In general, a loss of more than 20% of a muscles' mass is known to lead to reduced function and impaired muscle regeneration (4). In these serious cases the proliferation of fibroblasts can become excessive and therefore a deposition of scar tissue at the injury site can partially or fully obstruct muscle fiber regeneration (5). Moreover, scar tissue can limit the patient's ability to recover their pre- injury capabilities by causing inhibition of axonal ingrowth into the damaged area and thus reducing the contractile strength of the affected muscle (6). This delayed or even impairment of reinnervation can lead to severe atrophy of myofibers which can prevent future muscle reinnervation (7). TMI requires a surgical procedure to reconstruct the injured tissues, which is usually achieved using autologous muscle pedicle flap transplant into the affected area, although, in some severe cases of trauma the amputation of the injured limb may be warranted (8,9). This current medical intervention is not optimal since it is not always a possibility to acquire fitting grafts, while complications associated with transplantation make this treatment option challenging (9). There has therefore been an increased interest in using various natural or synthetic biomaterials to promote muscle regeneration. For these materials to properly support muscle differentiation there are some requirements that are provided in literature, such as various mechanical requirements and biological requirements. One of the most studied, and central biological requirements with a beneficial effect on muscle differentiation and thereby regeneration is the effect of alignment of a given scaffold (10–14). One of the currently used materials for skeletal muscle regeneration is decellularized tissues known as decellularized extracellular matrix (dECM). These require a donor of animal or human origin for the muscle material (15,16). These approaches are not without challenges, and problematic topics such as possible adverse immunologic response to implants still remain to be completely resolved (17). dECM can also be synthesized by the more easily obtainable human adipose derived stem cells (hASC). These cells are typically harvested during a liposuction (18) that could limit some of the challenges seen with decellularized organs. Therefore,

the aim of this study is to test the biological properties of ECM scaffolds derived from hASC to assess its suitability for skeletal muscle cell growth and differentiation in vitro.

## 1.2 Anatomy and Physiology of Skeletal Muscles

In the human body, skeletal muscles are a major component that make up approximately 40% of its total mass (12). The most well-known function of skeletal muscles is their ability to provide a mechanical force at the expense of chemical energy (ATP), however muscles are also known as contributors to metabolism serving as a storage for carbohydrates (sugars), various amino acids and maintaining the body's temperature. The mechanical force generates by the muscles can then be transmitted through the tendons and into the skeletal system where it can be translated into movement and maintenance of posture, which allows an individual to complete everyday activities and grants them a degree of autonomy. The muscle's structure can be seen as a series of parallel fibers organized as in a series of tubular bundles of decreasing size separated from each other by connective tissue; the epi-, peri- and endomysium, some containing blood vessels and nerves as seen in figure 1.

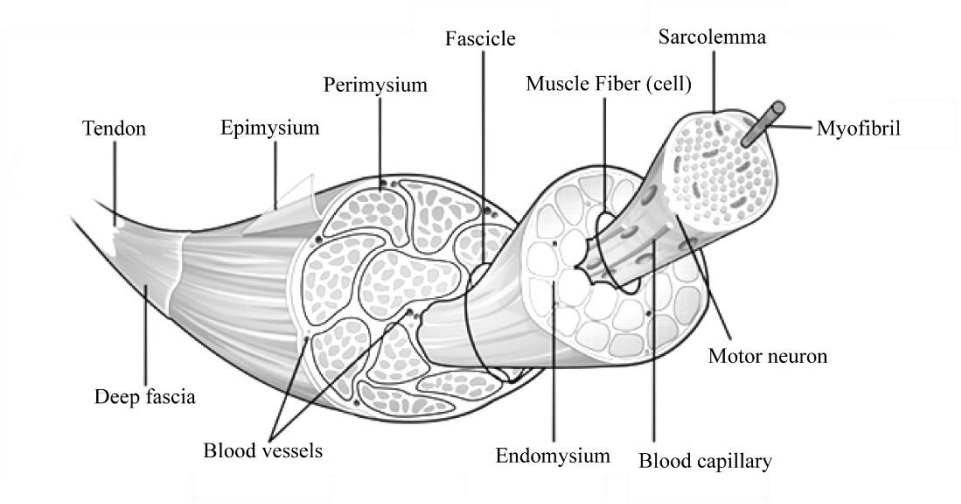


*Fig. 1: Schematic illustration of some of the key anatomical structures of the skeletal muscle* (67).

The functional unit of the skeletal muscle is the approximately 100µm thick multinucleated myofiber that consists of many bundles of myofibrils, themselves consisting of primarily myosin and actin, that are responsible for the contractile process. In brief, the contractile process is initiated after neuronal simulation of the myofiber causes a release of calcium ions from the sarcoplasmic reticulum. Due to the presence of calcium the protein troponin allows the dissociation of tropomyosin, and thereby exposing the myosin binding sites on the actin filament. This allows for attachment and sliding of the two filaments towards each other, leading to a contraction of the whole muscle in

unison. This force is transmitted into the tendon into the bone, that make e.g., the movement of an arm possible (12,19). When the homeostasis of the muscle is disrupted during various traumatic situations, certain important events take place to initiate regeneration of the affected area.

## 1.3 Skeletal Muscle Injury and Treatment

Traumatic muscle injuries can as be mentioned before stem from a variety of sources from traffic accidents to blast traumas. These injuries can be divided into three distinct categories (grade I-III) ranging from mild to most severe. Grade I comprise minor injuries such as bruises and sprains, these types of injuries do not cause any significant reduction of function. Grade II is considered moderate injury to the muscle where there is a noticeable loss of contractile force, and a formation of a local hematoma. The recovery period lasts form weeks to a month. Grade III is the most severe type of injury, where damage can extend to the whole section of the muscle and larger tears are often present. Recovery and rehabilitation for this grade takes months (20). For treatment options of grade, I-II in the acute treatment is typically the PRICE (Protection, Rest, Ice, Compression and Elevation) approach combined with the use of various nonsteroidal anti-inflammatory drugs (5). For grade III surgical interventions are typically needed to restore the muscle function. Furthermore, in these cases, volumetric muscle loss (VML) may be present which results in irrecoverable damage to the affected area due to a total loss of crucial elements such as the basal lamina and satellite cells and causes persistent inflammation and severe fibrosis at the injury site (21). VML is known for significant long-term disability in patients with high treatment costs and reduced quality of life (22). Treatment for VML usually involves autologous muscle transplant, but this option has limitations in terms of donor availability and transplant integration often preventing the employment of this treatment (21). Attempts to alleviate these issues have been made with the use of decellurized organ tissues of animal origin, which were theorized to be beneficial. This approach, however, proved not to be fully sufficient as challenges such as adverse immune reactions remain (17).

## 1.4 Skeletal Muscle Regeneration

From a microscopic perspective, when a muscle through, e.g., external force, suffers mechanical damage and the myofiber membrane is disrupted, it allows the flow of calcium inside of the cell resulting in cell lysis. With the release of intracellular components in the extracellular space, and general tissue damage at the injury site, inflammation is initiated, and an accumulation of circulating neutrophils into the damages tissues occurs within minutes. The neutrophils enhance the inflammatory response by the release of pro-inflammatory cytokines, such as tumor Necrosis Factor alpha (TNF-a) and Interleukin 6 (IL-6) that are then, in turn, able to recruit circulating monocytes and activate residual macrophages, while themselves able to phagocyte damaged cells and debris (23). Within the first 24 hours after injury many components of the local Extracellular matrix are degraded by protases and satellite cells, that are closely associated with the myofibers, become activated due to, e.g., the presence of various damaged-myofiber-derived factors (DMDFs) such as metabolic enzymes, and presence of cytokines such as IL6 (23–25). This activation causes a rapid increase in satellite cell proliferation, where some of these activated cells differentiate into myoblasts that migrate into the site of injury, while others remain and proliferate in their current from (23). The first steps of muscle regeneration begin around day 2-3 where myoblasts cell proliferation is reduced, and differentiation is increased after which myoblasts differentiate into myocytes and begin to fuse into myotubes aligning themselves according to architecture at the injury site. An overview of the differentiation process, together with myogenic marker expression, is presented in figure 2.

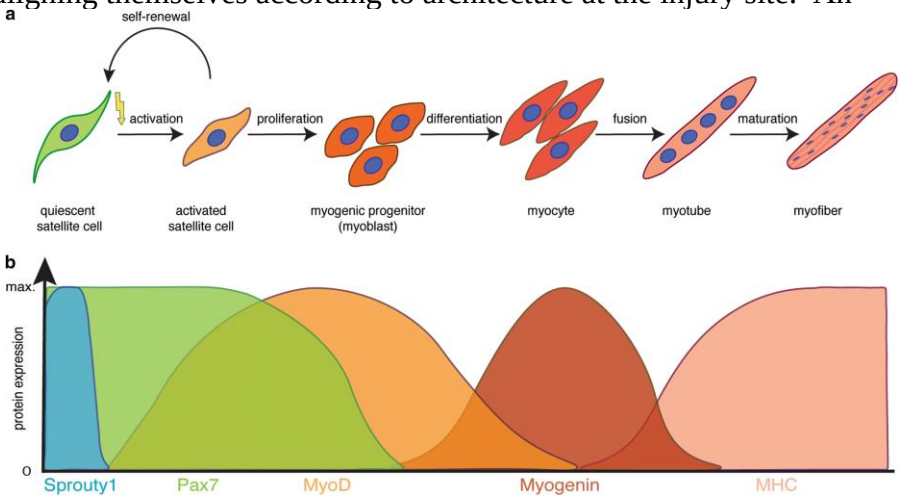


*Fig. 2: (a) Illustration of the skeletal muscle differentiation process form satellite cells to myofiber together with (b) the associated key myogenic markers* (68).

At around one week after injury, the regenerating muscle segments start to fuse with conserved tissue segments, thereby completing myofiber regeneration. To allow for muscle regeneration a suitable environment needs to be present, one of the known prerequisites are the cells' interaction with various molecules situated in the ECM designating it as a crucial factor for muscle regeneration (23).

## 1.5 The Structure of ECM in Skeletal Muscles and its Role in their Regeneration

In general, ECM is a multi-layered, three-dimensional material consisting of many different components, such as collagens, proteoglycans, polysaccharides, glycosaminoglycans and various growth factors in a highly interconnecting and dynamic environment. The ECM also allows the attachment of cells, gives tissue strength, stability, and plays an important role in tissue regeneration (26). In skeletal muscles, the ECM is highly aligned, which has proven to have an important positive effect on muscle differentiation, and regeneration (21,27,28). The skeletal muscle ECM is divided into different but interconnected layers with each surrounding different parts of the muscle structure, namely, epimysium, perimysium, and endomysium as described before. The brief overview of some of the individual proteins/molecules present in each layer can be seen on table 1.

| | **Location** | | |
|---|---|---|---|
| | Epimysium | Perimysium | Endomysium |
| **Components** | Collagen I | Collagen I, II, V, VI | Collagen I, II, IV, V |
| | Tenascin | Proteoglycans | Proteoglycans |
| | Fibronectin | Fibronectin | Fibronectin |

*Table 1: The presence of some of the ECM components according to their location in skeletal muscle ECM* (29).

Here the focus will be on only some ECM components primarily situated the endomysium as it is the layers that surrounds and supports the individual myofibers since its integrity dictates regeneration of a damaged muscle fiber and includes the stem cell niche (29). The ECM consists of two main classes of components, namely, fibrous proteins and proteoglycans. The most abundant fibrous proteins are collagens, elastins, fibronectins and laminins (26). Collagens be further categorized into different subtypes depending on their morphology, namely fibrillar (e.g. Collagen I, II, and III) or network forming (e.g. Collagen IV and VI) amongst others (29). The general structure of the fibrillar collagen consists of a triple helix made up of linked polypeptide chains. They can provide tensile strength, and aid in adhesion of cells. The most abundant collagen in muscle tissue is Collagen I that is important not only for its structural support of the ECM material, but also for its ability to promote migration and differentiation of myoblasts (30,31). An important network forming collagen is Collagen VI that has been shown to be a crucial component of the satellite cell niche since it regulates and maintains muscle regeneration (32). Its expression is very limited in myocytes, and therefore its deposition is dependent on the supporting MSC’s and the surrounding ECM

(29). Fibronectin is a short fibrillar protein that is deposited as disulphide-bonded dimers. It helps to align and fuse the myoblasts into myotubes during differentiation and also participates in cell adhesion and migration. Furthermore, the expression level of fibronectin can have an effect on activation and proliferation of satellite cells (26,29,33).

Decorin is a small proteoglycan that is present in all collagen containing tissues. It plays a critical role in the assembly of collagen fibers and is able to reduce muscle fibrosis by inhibiting TGF-β activity, and thereby plays a key role in both ECM assembly and muscle regeneration. The exact role of decorin in muscle differentiation is still under investigation (34). Apart from its various components the ECM is also able to release various cytokines as FGF2, HGF, and SDF-1 that are able to positively affect the proliferation of myogenic progenitor cells, by the induction of the transcription of among others MyoD and Myogenin genes in the progenitor cells (35). To deposit the ECM material, mesenchymal stem cells may be used, one of them being the hASC's which possess this potential for ECM synthesis (36).

## 1.6 Adipose Derived Stem Cells

Human adipose derived stem cells (hASC) are a subset of mesenchymal stem (MSC) cells with the ability to differentiate into the various cell linages, and thus able to differentiate into cells such as keratinocytes, endothelial cells, and fibroblasts while possessing similar regenerative properties as other MSC's. Due their abundant presence in the human body inside white adipose tissue, their extraction can easily be conducted with the use of the minimally invasive liposuction procedure and can therefore be used in autologous transplantation (37). These cells have yet not been ascribed as specific surface marker making them a heterogeneous population (36). The hASC's are capable of the secretion of various ECM components such as collagen I, VI and fibronectin (fig. 4) that can provide a combination of enhanced proliferation, migration, and differentiation capacity of muscle myoblasts (18,29–33,38). In wound healing the hASC derived ECM plays an important role in the reduction of fibrosis and thereby tissue scarring (39). In other areas such as bone and cardiac tissue engineering ECM has also shown a positive effect on regeneration, and cell differentiation (40,41). As described, the ECM plays and important role in muscle regeneration, and to enhance its deposition, the use of macromolecular crowder will be employed. The effect of the macromolecular crowder ficoll has shown to increase ECM deposition by accelerating biochemical reactions, such as the synthesis of ECM components in the culture environment (42,43).

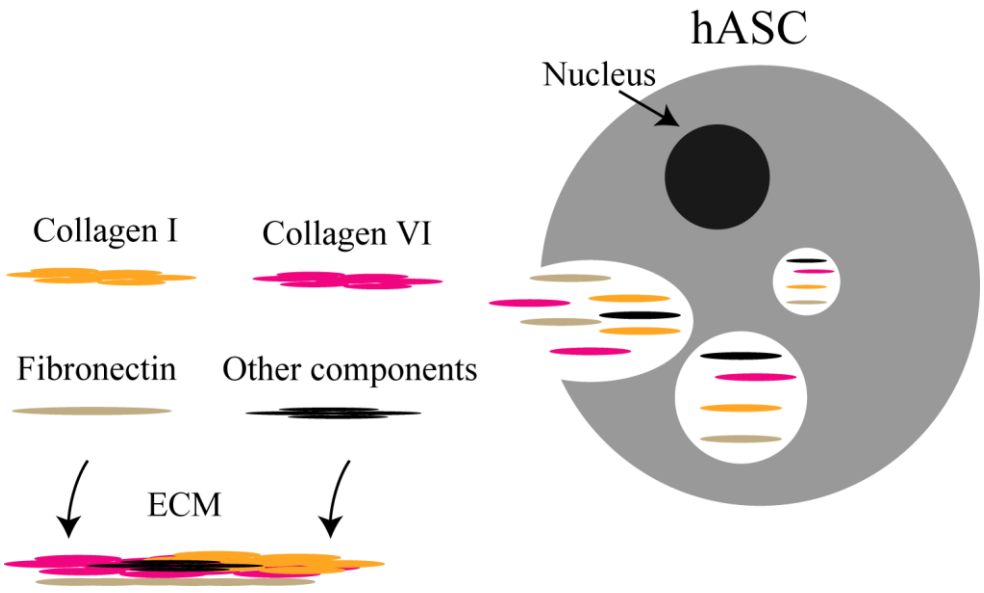


*Fig. 4: Illustration of some of hASC's ECM production capacity including Collagen I, VI and fibronectin.*

## 1.7 Aim and hypothesis

The use of ECM has the potential to be favorable for muscle regeneration due to the presence of various beneficial components. One of the key factors with important influence on muscle regeneration apart from the ECM itself is the alignment of the substrate. Therefore, the aim of this study is to investigate the effects of aligned or randomly oriented ECM derived from hASC on the growth and differentiation capacity of the C2C12 cell line. Based on the previously presented literature we hypothesize that anisotropic ECM scaffolds have a positive effect on muscle differentiation due to their influence on cell alignment and maturation.

# 2. Methods

## 2.1 Culture Environment and Cell Seeding

The human adipose derived stem cells (hASC) used in this project were sourced and isolated from a voluntary donor while undergoing elective liposuction. The details and ethical approval for this procedure has been described previously (18). The C2C12 murine myoblast cells were purchased form ATCC, while the HSMC were acquired from Cook MyoSite. The cryopreserved cells were thawed in a water bath at (37 °C), hereafter the solution was transferred to a centrifuge tube and resuspended with culture medium. The tube was centrifuged for 5 min at 1200 RPM (Hettich Rotina48 R) at room temperature for pellet formation. After decanting and counting, the cells were transferred to a T175 flask for culture. The hASC's and C2C12 cells were cultured in Dulbecco's Modified Eagle Medium (DMEM) (DMEM - high glucose, no pyruvates, Gibco supplemented with 10% Fetal Calf serum (FCS) and 1% streptomycin/penicillin solution (100 IU/ml penicillin, 0.1mg/ml streptomycin Thermo Fisher). The primary human skeletal muscle cells (HSMC) were cultured in Ham's F12 medium (Ham's F-12 Nutrient Mix, Gibco) supplemented with the following: 0.1% human insulin (10mg/ml, Sigma Aldrich), 0.1% dexamethasone (0.4 mg/ml, Sigma Aldrich), 10% FCS, 1% penicillin/ streptomycin (100 IU/ml penicillin, 0.1mg/ml streptomycin, Thermo Fisher) and 0.5% gentamycin (10mg/ml, Invitrogen). Additionally, immediately before use the F12 medium was supplemented with 0.1% EGF (human, recombinant, 10µg/ml, Sigma) and 0.01% FGF-β (human, recombinant 10µg/ml, Gibco).

To maintain the culture, the medium was replaced, in a class II LAF-bench (Holten Laminair), with fresh, warm (37 °C) growth medium every other day. The cells were stored in the incubator (Steri-Cycle CO2 Incubator, Thermo Scientific) at 37 °C and 5% CO2.

For culture passaging, the media was first removed and then the surface washed with PBS. Next TrypLE (Gibco) was added, and the flask incubated for five min until the cells were visibly floating in suspension when observed under a microscope. After the detachment, the flasks surface was washed multiple times with media to ensure complete cell removal. The cell suspension was then centrifuged for 5 min at 1200 RPM at room temperature. The cell pellet was resuspended in culture media.

### 2.1.1 Optimization of hASC Seeding Density

Presto blue (Invitrogen) was used to assess the optimal seeding density for hASC's. In brief, Presto Blue contains resazurin that is reduced to resorufin a highly fluorescent molecule, while also producing a pronounced color change in the media proportional to the cell population/ metabolic activity. The evaluated cell concentrations were 2.000, 4.000, 6.000 and 8.000 cells/ $cm^2$. One tenth of the well's media volume was added in form of the Presto Blue reagent. The cells were incubated for 10 min in an incubator at 37 °C. The solution was transferred to a clear 96 well plate (Corning) in duplicates. Hereafter the absorbance at 570 nm was measured with a multiplate reader (EnSpire Multimode Plate Reader, PerkinElmer) at 24, 48 and 36 hours after seeding.

## 2.2 Culture Plate Coating and ECM Production

The culture plates consisted of three groups: a group made up of smooth bottom 24 well plates (Corning) (control), 24 well plates with aligned surfaces (aligned group) (Nanofiber Solutions) and 24 well plates with randomly orientated surfaces (random group) (Nanofiber Solutions) were all coated with poly-dopamine to ensure an optimal attachment surface as described below. To each well a 50mM NaOH solution was added and incubated for 10 min. Hereafter the solution was removed and the wells were incubated for 10 min with MES buffer (9.76% MES-free acid (Merck) in water adjusted to pH 6 with NaOH) and washed with sterile MiliQ water. Next, 1mg/ml dopamine hydrochloride (Sigma Aldrich) in TRIS base buffer (12% TRIS base (Merck) in water adjusted to pH 8.5 with HCL) was filtered through a 0.22µm syringe filter. This solution was added to each well and incubated for one hour at room temperature. Lastly the poly-dopamine solution was removed, the wells washed with sterile MiliQ water and were let to airdry overnight. After 24 hours of culture the cells were induced for ECM production with DMEM supplemented with 20 mM sterile Ascorbic acid solution (Sigma) (1:100) and 9% Ficoll solution (Ficoll 70 (Cytiva): 18.75 mg/ml and Ficoll 400 (Cytiva): 12.50 mg/ml). The ECM was produced for 10 days.

## 2.3 ECM Structure Assessment

### 2.3.1 Qualitative and Quantitative Collagen Fiber Assessment

To assess the capability of ECM production by the hASC the Sirius Red fast green dye (Chondrex) kit was used to visualize the collagenous (stained red) and non-collagenous fibers (stained green) for microscopy and assessment of collagen concentration. Before staining the growth media was removed and the wells were washed with PBS. Pre-heated (37 °C) extraction buffer (1% Triton X-100 and 20mM ammonium hydroxide in PBS) was added to each well, and incubated for 5 min in a heat chamber at 37 °C. The buffer was removed, and the wells were washed with PBS before being transferred to a horizontal shaker (IKA HS 50) for 20 min at room temperature. Next, Khale fixate (60% distilled water, 28% ethanol (95%), 10% formaldehyde (37%), 2% glacial acidic acid) was added to each well and incubated for 10 min at room temperature. After fixation the fixative was removed, and each well was washed with PBS. For the staining, the PBS was removed, and staining solution added. The samples were incubated at room temperature for 30 min. Hereafter the solution removed, and the wells washed thoroughly with demineralized water whereafter the plates were observed under an inverted microscope (Primovert, Carl Zeiss). Hereafter 1 ml of extraction buffer was added, and each well was washed with it until no color was visible in the sample. This liquid was then transferred into a black, clear bottom 96 well plate (Corning) and the optical density (OD) at 540 nm and 605 nm was read on the spectrophotometer (EnSpire Multimode Plate Reader, PerkinElmer). The calculation of the collagen amount in each well was performed according to the manufacturer's instructions (Chondrex). In summary: To calculate the concentration of collagen in each well, it is necessary to correct for the contribution of fast green to OD 540 value of collagen. This is done by subtracting 29.1% of the OD 605 value from it and then dividing by 0.0378 which is the color equivalence (OD values/µg protein) for collagen resulting in the following formula:

$$collagen\ (\mu g/\ well) = \frac{OD\ 540\ value - (OD\ 605\ value \cdot 0.291)}{0.0378}$$

### 2.3.2 Assessment of Specific ECM Constituents

Indirect immunofluorescent standing was chosen to specifically visualize three components of the ECM, namely Collagen I, Collagen VI, and fibronectin.

The cells were fixated with a 4% formaldehyde solution for 15 min. Hereafter a blocking solution consisting of 1% bovine serum albumin in PBS (BSA- PBS) was added and incubated on samples for 30 min. The blocking solution was removed and a BSA-PBS solution with primary antibodies was added. The primary antibodies were diluted 1:200 in BSA-PBS consisted of the following: anti-Collagen Type I antibody produced in mouse (C2456, Sigma-Aldrich), anti-fibronectin antibody produced in rabbit (F3648, Sigma Aldrich) and anti-collagen VI Antibody produced in rabbit (SD83-03, Invitrogen). The antibodies were incubated overnight at 4°C. After the incubation the primary antibody was removed and the secondary antibodies were diluted 1:500 in BSA-PBS consisted of the following: Alexa Fluor 488 donkey anti-mouse (A21202, Invitrogen) and Alexa Fluor 555 goat anti-rabbit (A21428, Invitrogen) for the control samples, while for the aligned and random groups the secondary antibodies were Cy5 goat anti mouse (124S, Chemicon) and Cy5 goat anti rabbit (132S Chemicon). The images were captured using a Axio observer Z1 (Carl Ziess) inverted microscope with a digital camera (Hamamatsu Orca Flash 4.0)

## 2.4 Skeletal Muscle Cell Seeding and Differentiation

Before seeding, the ECM was DNase treated by diluting DNase 25 stock solution (100UI/ml in PBS) (Sigma Aldrich) 1:10 in sterile DNase working solution (5% 0.1M MgCl, 0.65% $CaCl_2$ in PBS). The solution was incubated for 30 min at 37 °C, washed with PBS and left overnight on an orbital shaker (The Belly Dancer, Stovall Life Science) at low RPM.

The treated decellularized plates were hereafter UV sterilized (UV Stratalinker 1800, Stratagene) for 5 min with lids on to ensure a suitable culture environment. Whereafter C2C12 cells and HSMC were seeded onto the plates at 20.000 cells/$cm^2$. The C2C12 cells were grown in DMEM and the HSMC were cultured in Ham's F12 medium as described previously. Both cell groups were cultured until a high confluence was reached whereafter differentiation would be induced. For both cell lines the differentiation media consisted of DMEM supplemented with 2% FCS 1% penicillin/ streptomycin and 0.5% streptomycin. The cells would be allowed to differentiate for seven days.

## 2.5 Assessment of Skeletal Muscle Differentiation

### 2.5.1 Immunofluorescence

For the indirect immunofluorescent staining of the muscle cells the same protocol was employed as described in section 2.3.2 however with the following changes:

The cells were permeabilized using a 0.3% triton X-100 in PBS solution (Sigma Aldrich) for 10 min after the fixation step. The primary antibody was anti myosin heavy chain (skeletal) produced in mouse (M1570, Sigma Aldrich), while the secondary antibody was Cy5 goat anti mouse (124S, Chemicon). To visualize the nuclei of the cells Hoechst 33342 (Invitrogen) was used as described in the following: The Hoechst staining solution was diluted 1:2000 in PBS and added to empty wells. The samples would be incubated for 10 min in the dark, whereafter the staining solution would be removed, and the wells washed with PBS.

The samples would be observed using the same equipment as the ECM in section 2.3.2.

### 2.5.2 Giemsa staining

To visualize the gross structure of the myotubes, Giemsa staining was performed. The Giemsa dye stains basophilic cytoplasm blue and nuclei purple.

The Giemsa staining solution was prepared by diluting the Giemsa stock solution (Sigma Aldrich) 1:20 in a 10mM phosphate buffer (0.2 M $Na_2HPO_4$ and 0.2 M $NaH_2PO_4$ in water). The differentiation media was removed, and the cells fixated with cold (-20°C) methanol (100%) for 5 min after which the fixative was removed, and the wells were air dried for 10 min. Giemsa solution was added to the wells and incubated for 45 min at room temperature. After the incubation, the surplus solution was washed with distilled water and observed under the microscope (Primovert, Carl Ziess).

## 2.6 Assessment of the Expression of Target ECM Genes

### 2.6.1 RNA extraction

Firstly, all media was removed from the wells and washed with PBS. Hereafter the wells were thoroughly rinsed with 350 µL of RNA lysis solution (Bio-Rad). Liquid form each well was then transferred to a separate 1.5 ml Eppendorf tube together with 350 µL of 70% ethanol. The samples were stored at -80°C.

### 2.6.2 RNA Isolation

The RNA purification was performed Aurum Total RNA Mini Kit (Bio-Rad). After thawing the samples were transferred into RNA-binding columns situated in 2ml capless tubes. All the samples were centrifuged for 1 min at 12,000g. The filtrate was discarded and 700 µl of low stringency solution was added and the samples centrifuged as before. Next, 700 µl high stringency solution was added to each column and centrifuged. One more time, the low stringency solution was added to each column followed by centrifugation for first 1 min, and after the removal of the filtrate centrifuged for 2 additional min. Hereafter the columns were transferred to 1.5 ml capped tubes and 40 µl of preheated elution solution (70°C) was added to the columns filter stack and incubated for 2 min at room temperature before being centrifuged for 2 min. The columns where hereafter discarded, and the purity and quantity of the isolated RNA was assessed with the use of a nanodrop spectrophotometer (DS-11 FX,  DeNovix) and then stored at -80°C.

### 2.6.3 cDNA synthesis

The cDNA synthesis was conducted using the iScript cDNA Synthesis Kit (Bio-Rad). All the samples were firstly normalized to the lowest concentration of RNA in given samples. Then, a master mix made up of 4 µl of 5X iSCRIPT reaction mix and 1 µl of iSCRIPT reverse transcriptase was added to each of the samples. These were hereafter transferred to a thermal cycler (T100 Thermal Cycler, Bio-Rad). The cDNA synthesis protocol was as follows: 25℃ for 5 min, 42℃ for 30 min, 85℃ for 5 min, and lastly at 4℃ until sample collection. The cDNA samples were stored at - 80℃.

### 2.6.4 Primer Optimization

Multiple primers for Collagen I alpha 1 and decorin (Biosearch Technologies) were optimized to find the most suitable annealing temperature. In brief, each primer Cq was measured at different annealing temperatures ranging from 59-65 ℃ together with negative controls for each temperature. The primer pair with the lowest Cq value in the temperature range 60-62 ℃, with uniform melt curves were chosen for sample analysis.

### 2.6.5 Quantitative Polymerase Chain Reaction Procedure

All the samples were firstly diluted 1:100 with RNAse-free water and vortexed. For each gene analyzed, a mastermix consisting of forward primer, reverse primer, and SYBR green (iTaqTM Universal SYBR Green Supermix, Bio-Rad). Sample and master mix was loaded into a hard-shell 96 well plate (Bio-Rad) in duplicates together with standards and no template controls. Henceforth, the plate was sealed using an optical clear film (Bio-Rad). Next, the plate was centrifuged at 1,200 RPM for five min before the transfer to the qPCR instrument (CFX-connect, BioRad). The qPCR for all the samples were as follows: activation step at 95℃ for 5 min, followed by 40 cycles of denaturation at 95℃ for 15 sec and an annealing step, with annealing temperatures and primer sequences presented in table 2, for 30 sec. The melt curves were run from annealing temperature to 95℃.

| **Gene Symbol** | **Gene Description** | **Primer sequence (5'-3')** | | |
|---|---|---|---|---|
| | | Forward primer | Reverse primer | Annealing temperature |
| COL1A1 | Collagen I alpha 1 | CTTGGATGCCAAAGTCT | AATCCATCGGTCATGCTCTC | 62 ℃ |
| COL6A1 | Collagen VI alpha 1 | CGTGGACCTGTTCTTTGTGC | GTTTCGGTCACAGCGGTAGT | 62 ℃ |
| Fn | Fibronectin | ACCTACGGATGACTCGTG CTTTGACAAAGC | CAAAGCCTAAGCACTGGC ACAACA | 62 ℃ |
| DCN | Decorin | CTTTCCACACCTGCAAACTCT | GAGGATGATAGTGGCCTTCA | 62 ℃ |
| PPIA | Peptidylprolyl Isomerase A | TCCTGGCATCTTCTCCATG | CCATCCAACCACTCAGTCTTG | 62 ℃ |

*Table 2: List of primers sequences used for the qPCR procedure: Collagen I alpha 1, Collagen VI alpha 1, Fibronectin, Decorin and Peptidylprolyl Isomerase A with their respective annealing temperatures.*

## 2.7 Statistics

All data were assumed to be normally distributed, therefore parametric tests were used to analyze the data. Nonparametric tests have a lower power and using them to analyze normally distributed data would lead to a larger p-value and thereby misleading interpretation.

A One-Way ANOVA was used to compare the quantitative results from eluded dyes in the Sirius Red/Fast Green assay and to compare differences between groups in the semi-quantitative reverse transcriptase qPCR (RT-qPCR) procedure. The relative gene expression for RT-qPCR data was calculated using the Pffaffl method to determine the gene expression in the test and control samples. Error bars indicate standard deviation. All statistical analysis was performed using IBM Statistics SPSS 27 software with the significance level set to 95%.

# 3 Results

## 3.1 Evaluation of ECM

### 3.1.1 Optimization of hASC Seeding Density

Presto Blue was used to evaluate the optimal seeding density, while Sirius Red/ Fast Green was used to qualitatively evaluate the presence of collagenous fibers (fig. 5 a-b). Sirius Red binds to the helical structure of various collagens staining the fibers red while Fast Green binds to non-collagenous fibers.

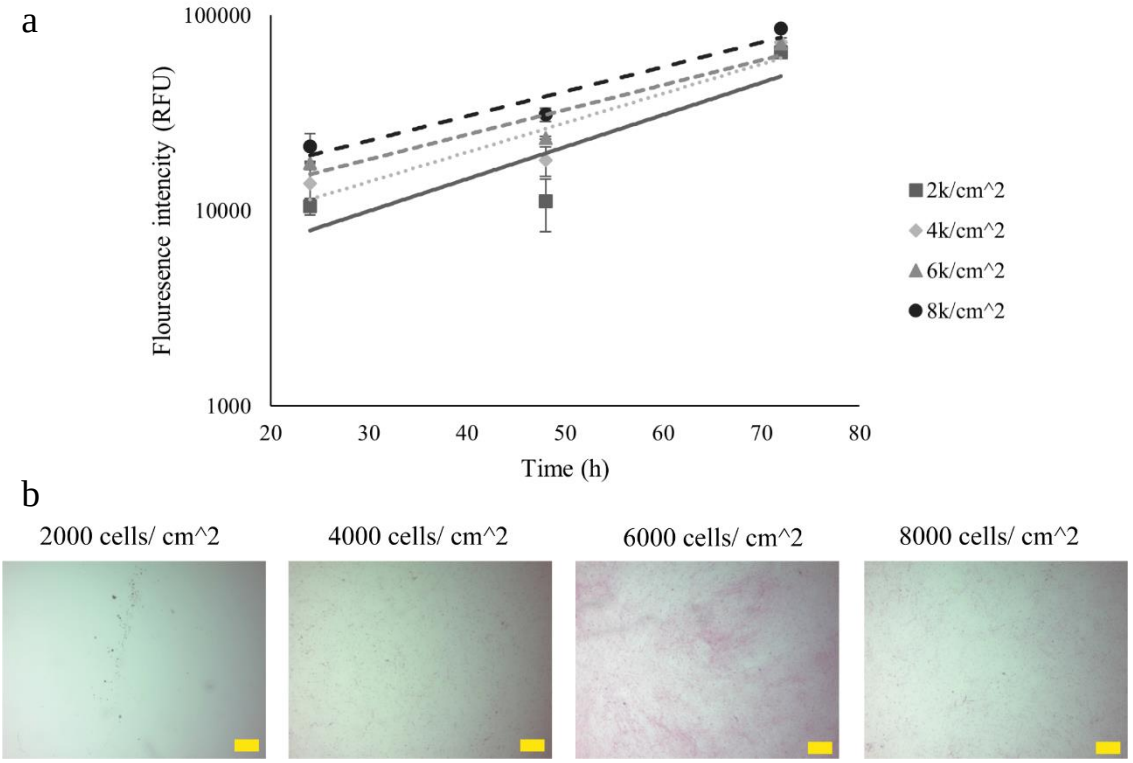


*Fig. 5: (a) Illustration of cell proliferation over three days with regression equations shown and (b) collagenous fiber evaluation for four cell seeding densities: 2000, 4000, 6000 and 8000 cells/cm$^2$. Bar: 200 µm.*

The doubling times for all groups were analyzed. The groups had the following doubling times: 2000 cells/cm$^2$: [15 (1)], 4000 cells/cm$^2$: [20 (3)], 6000 cells/cm$^2$: [23 (0.5)] and 6000 cells/cm$^2$: [23 (0.6)] hours. The presence of collagenous fibers was assessed qualitatively in the different seeding densities. Here it can be seen that the 6000 cells/cm$^2$ group appears to have more collagenous fibers when compared to the other groups. Based on the above, a 6000 cells/cm$^2$ seeding density has been used for hASC seeding, a compromise between proliferation rate and collagenous fiber production.

### 3.1.2 Qualitative and quantitative assessment of ECM collagen presence

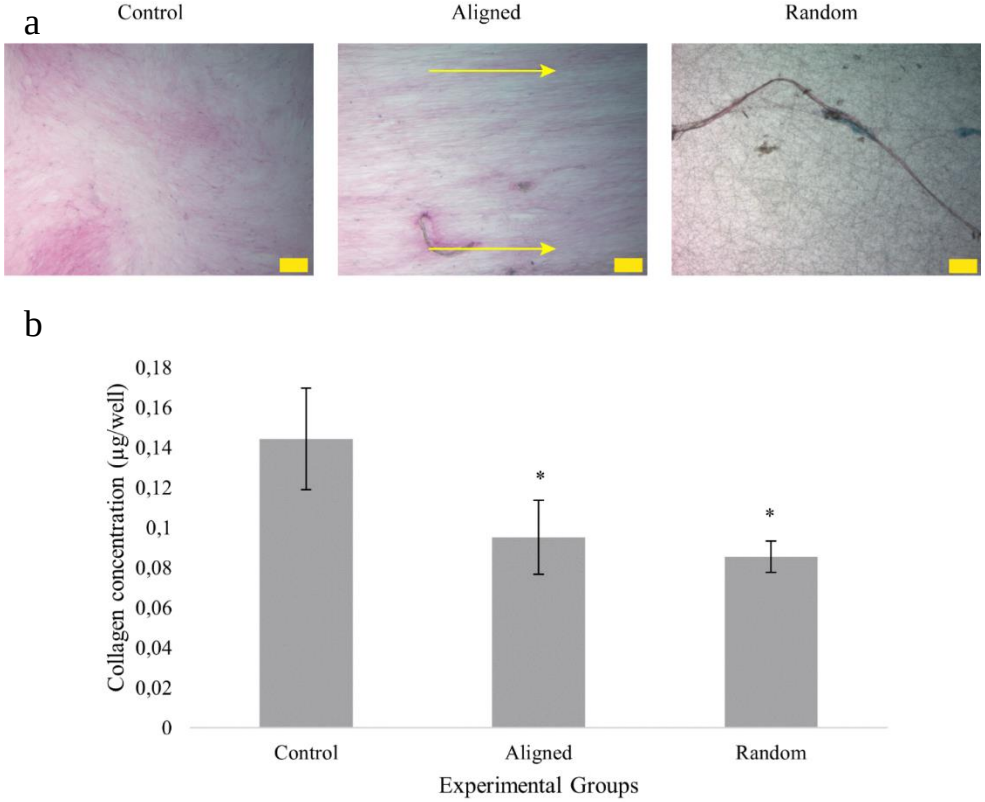


*Figure 6: Results of the Sirius Red/ Fast Green staining on ECM at 40x magnification for the three groups (a) and the subsequent qualitative analysis of collagenous fibers (µg/well) (b) . *: significant versus control. Yellow arrows indicate alignment. Bar: 200 µm.*

The ECM on the aligned substrate show more lightly stained areas. It also appears that there are more patches with insufficient ECM coverage compared to the control (Fig. 6.a). The fiber orientation seems to follow the underlying substrate (yellow arrows). Lastly, the ECM in random orientated substrate group appears to be the least prominent when compared to the other two groups with a very thin layer of ECM observed. However, in this group, a larger presence of non-collagenous aggregates is observed. The fiber orientation of this group cannot be fully assed but are assumed to be randomly oriented. Fig. 6.b illustrates the quantitative analysis of the eluted Red/Fast Green dye representing the measured collagen concentration per well in the three. A statistically significant decrease in the concentration of collagen is noted between the control group and both the aligned [0.095 (0.018)] µg/well vs. [0.144 (0.025)] µg/well and randomly orientated [0.085 (0.007)] µg/well vs. [0.144 (0.025) µg/well] substrate.

### 3.1.3 Targeted visualization of ECM components

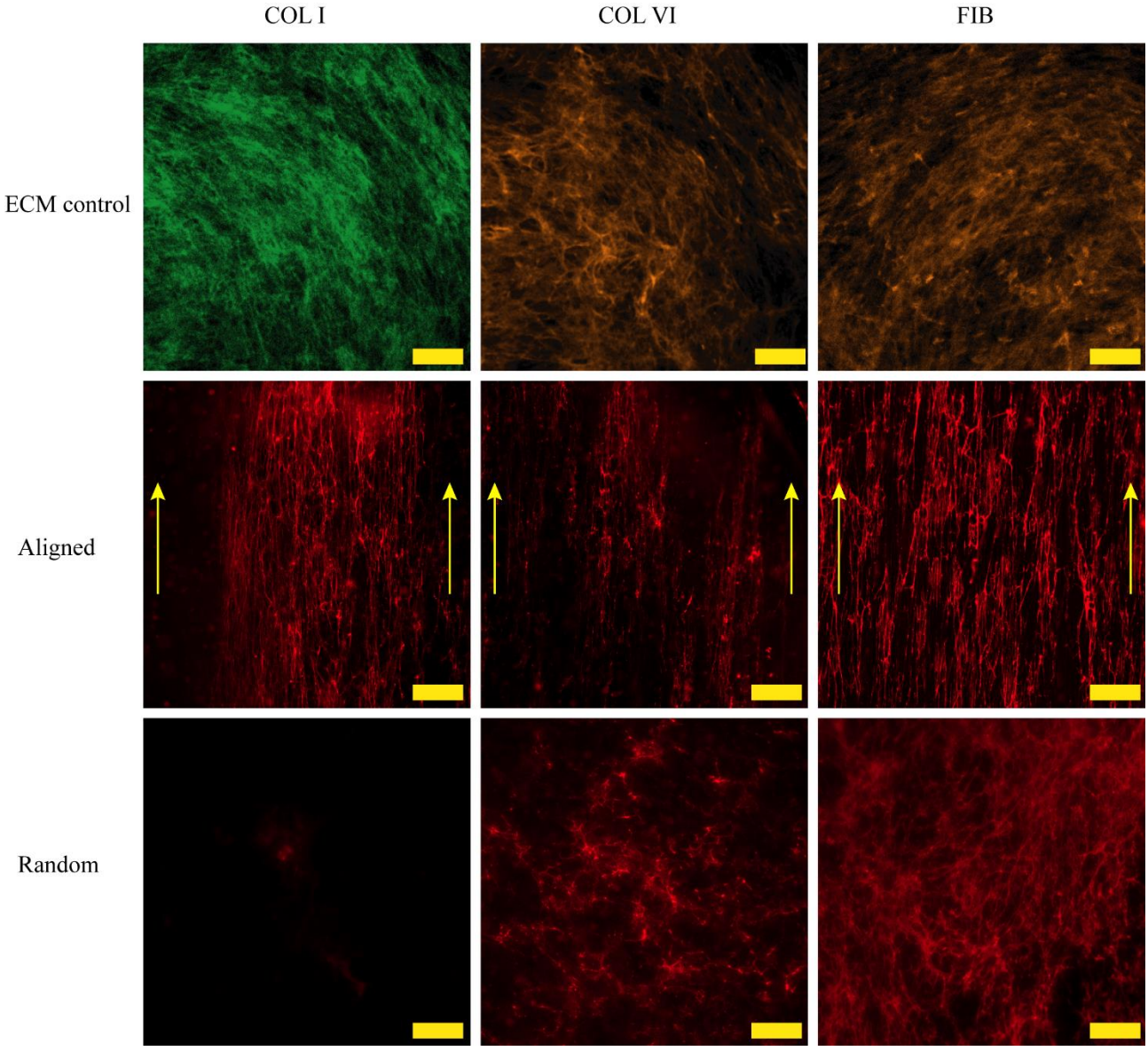


*Fig. 7: Illustration of the immunofluorescent staining for collagen I, collagen VI, and fibronectin in the three groups: control, aligned and randomly orientated at 200x magnification. Bar: 100 µm*

When analyzing figure 7 it can be said that generally, the presence of the targeted ECM molecules appears to be reduced in both groups, when compared to control. The aligned group seems to possess aligned ECM fibers in contrast to the other groups. Further elaboration below.
Looking at the aligned group it can be observed that the overall presence of collagen I, VI and fibronectin appears overall reduced, and their coverage of the surface is patchier in nature The fibers themselves appear thinner and more finely branched than the control. However, all the protein fibers in the aligned group seem to follow in parallel to the underlying scaffold material creating an

aligned pattern. The most intense signal comes from the aligned fibronectin which appears to cover more of the underlying substrate compared to collagen I and VI. The random group expresses similar differences regarding in fiber amount, thickness, and coverage. However, the fibers lack the alignment as observed in the previous group. Fibronectin is also well distributed and prevalent, but collagen I appears to be the least prevalent when compared to both the control and aligned group.

### 3.1.4 Transcriptional activity of ECM genes

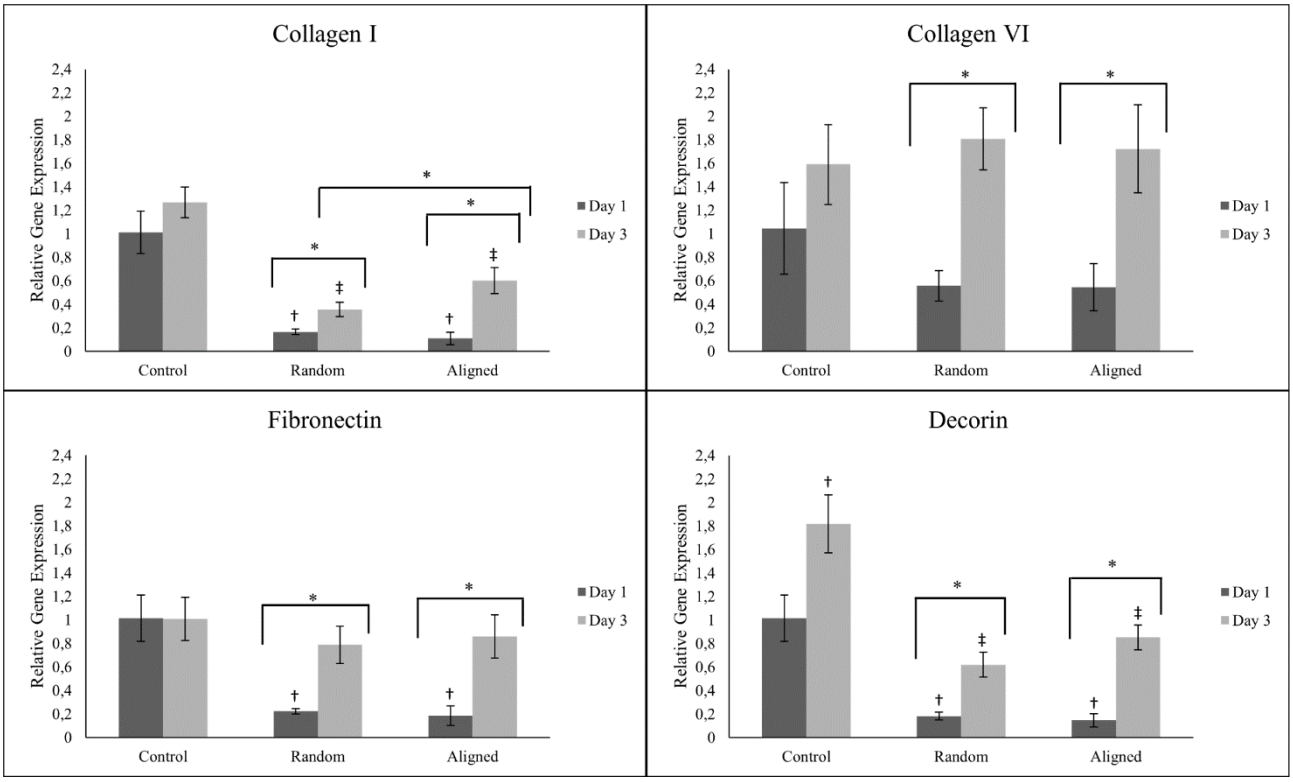


*Figure 8: the normalized relative gene expression of target genes (collagen I, collagen VI, fibronectin and decorin) in the control and experimental groups at day 1 and 3. †: Significance vs control day 1, ‡: Significance vs. control day 3, *: significance between target groups.*

Looking at figure 8 it is apparent that in general all ECM genes have a statistically significantly reduced expression at day 1 while collagen I and fibronectin also have a significant reduction in ECM expression at day 3 when compared to control. Generally, there is a significant increase in expression in some of the selected genes between day 1 and 3 in the aligned and random groups. Complete analysis follows.

Collagen I: In the random group there was a significant increase in the expression of the gene between day 1 and day 3 [0.166 (0.022)] vs [0.357 (0.060)]. However, their expression was significantly lower than of both control day 1 and day 3. For the aligned group there was a significant

increase of gene expression between day one and day three [0.110 (0.052)] vs [0.601 (0.111)]. There was also a significant increase in gene expression between day 3 in the random group and day 3 in the aligned group [0.357 (0.060)] vs [0.601 (0.111)].

Collagen VI: For the random group there was a significant increase in the expression of the gene between day 1 and day 3 [0.557 (0.128)] vs [1.807 (0.263)]. For the aligned group there was a significant increase of gene expression between day 1 and day 3 [0.545 (0.200)] vs [1.721 (0.374)].

Fibronectin: in the random group there was a significant increase in the expression of the gene between day 1 and day 3 [0.222 (0.024)] vs [0.789 (0.159)]. The expression at day 1 in the random group was also significantly lower than the expression in the day 1 control group. For the aligned group there was a significant increase of gene expression between day 1 and day 3 [0.186 (0.081)] vs [0.860 (0.183)].

Decorin: For the random group there was a significant increase in the expression of the gene between day 1 and day 3 [0.182 (0.032)] vs [0.620 (0.105)] the expression at day 1 and 3 in the random group was also significantly lower than the expression in the day 1 and 3 control group. For the aligned group there was a significant increase of gene expression between day 1 and day 3 [0.146 (0.056)] vs [0.853 (0.105)].

## 3.2 Evaluation of Muscle Differentiation

### 3.2.1 Visualization of Myotube Structure of the C2C12 Cells

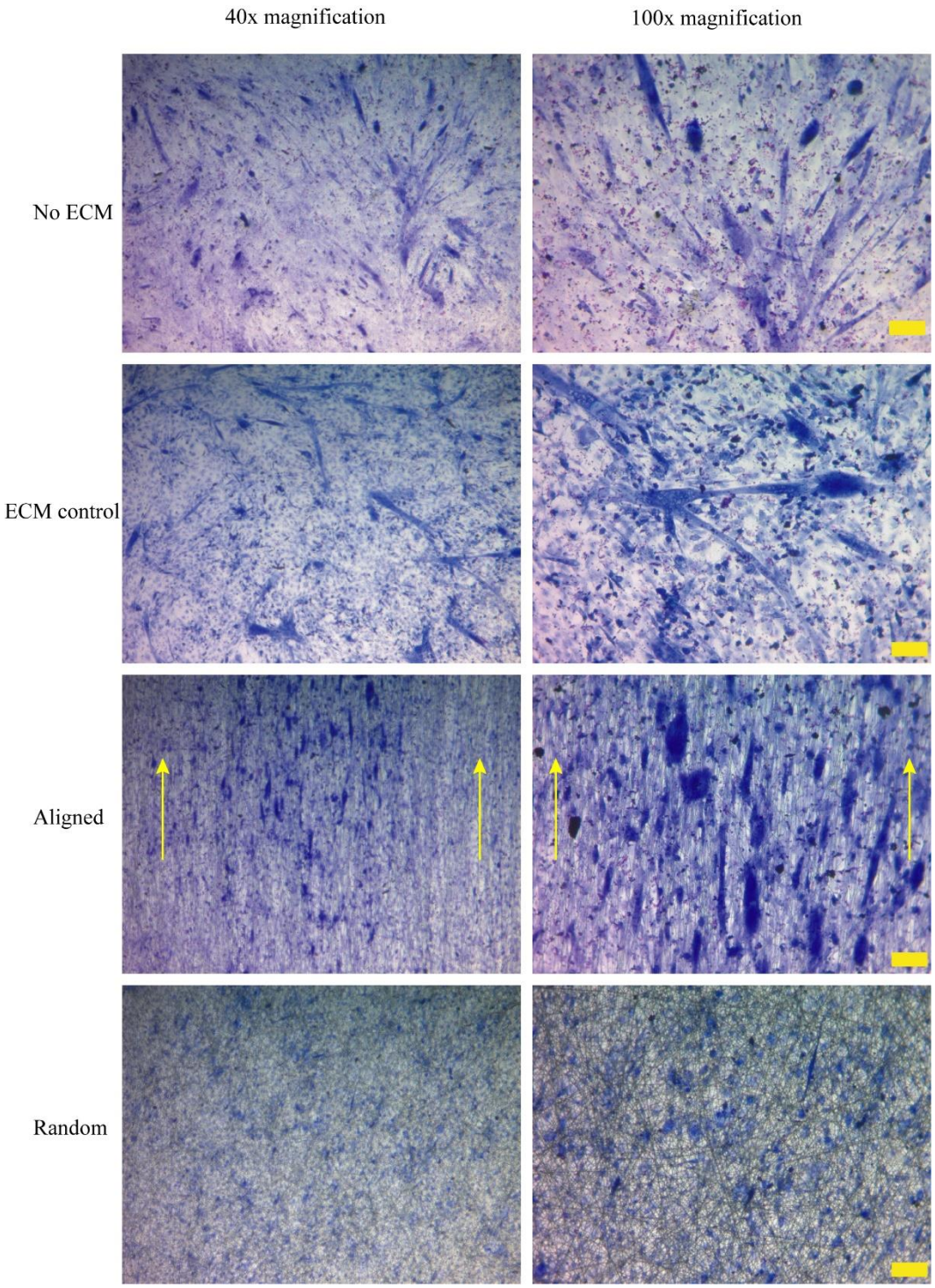


*Fig. 9: Illustration of the Giemsa staining on myotubes of C2C12 present in the different control and experimental groups: ECM control, Aligned and random organized substrates at 40x and 100x magnification. Arrows indicate alignment. Bar: 100µm*

Looking at the aligned group  and comparing it to the control ECM and no ECM groups (fig.9)  it can be observed that the myotubes are in general thinner, shorter and posses fewer fused nuclei, but appear slightly more stained. They seem to be aligning themselvs in parallel with the underlying substrate (yellow arrows).

When assessing the myotubes in the random orientated group compared to the two control groups, it is apparent that the presence of myotubes is reduced, and the myotubes observed are sporadic and noticibly thinner.

### 3.2.2 Targeted Visualization of C2C12 Differentiation

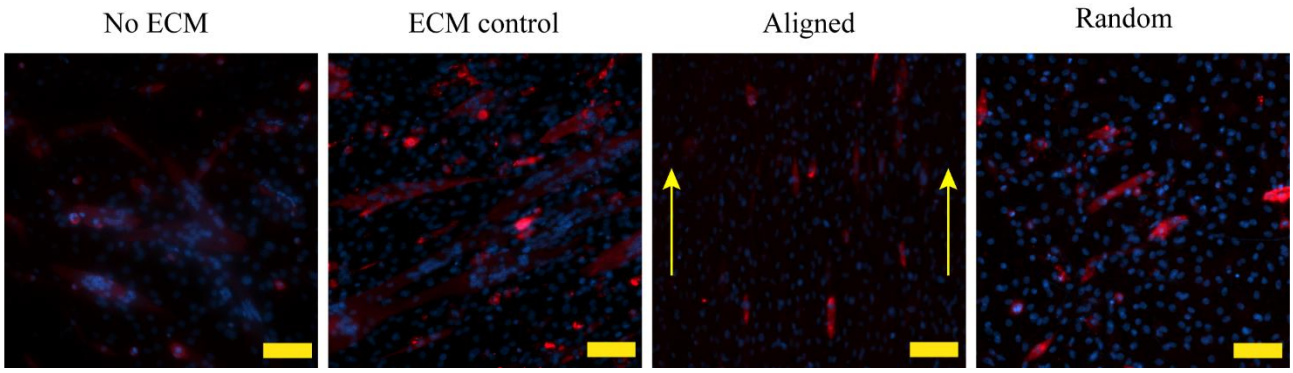


*Fig. 10: Illustration of the immunofluorescent staining for myosin heavy chain (red) and nuclei (blue) in the control ECM, Aligned, ECM control, ECM on aligned substrate, ECM on Random orientated substrate and No ECM groups. Arrows indicate alignment. 200x magnification. Bar: 100 µm*

Looking at the aligned ECM group versus the no ECM group and ECM control group (fig. 10) the myotubes appear much fewer in number, and thickness compared to both groups. Furthermore, the number of nuclei in the myotubes is visibly lower than the other two. The myotubes in the random aligned group similarly to the aligned group have thinner, fewer, and less nucleated myotubes when compared to both the no ECM group and the ECM control group with the difference that here they appear to be randomly orientated. The red color indicating presence of MyoH is present in all the groups which suggests that the cells are differentiated.

## 3.3 Pilot study: Assessment of hSKMM Differentiation on ECM

To elucidate the differentiation of another cell type on ECM a conducted a pilot study was conducted. Here the differentiation of primary hSKMMs on ECM was analyzed.

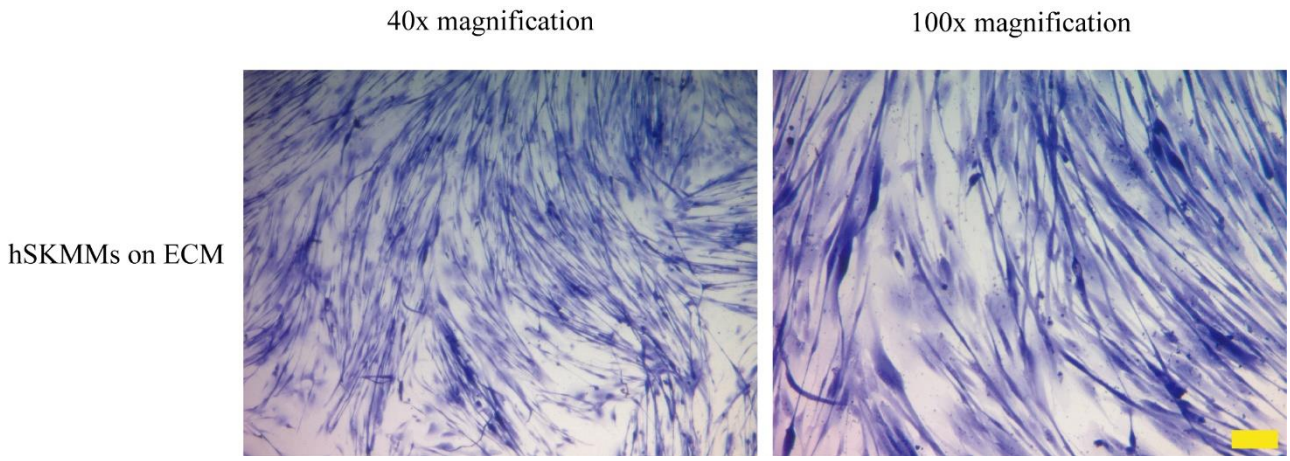


*Fig. 11: Illustration of the Giemsa staining on myotubes of hSKMMs on ECM at 40x and 100x magnification. Bar: 100 µm*

It appears that the hSKMMs grown on ECM are well differentiated with long multinucleated myotubes present. The myotube density appears to be high (fig.7).

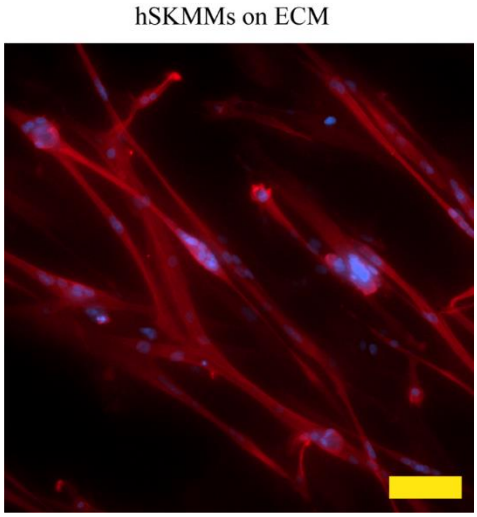


*Fig. 12: Illustration of the immunofluorescent staining for myosin heavy chain (red) and nuclei (blue) in the control ECM and hkSMMs on ECM group. 200x magnification. Bar: 100 µm*

On Figure 12 the HSMCs appear to be elongated, and multinucleated myotubes indicates differentiation. The high presence of myoH further supports differentiation.

# 4. Discussion

The efficacy of hASC derived ECM on muscle regeneration has been studied only to a limited extent in the literature. Therefore, the purpose of this study was to investigate the influence of ECM on skeletal muscle cell differentiation and to assess the effect of an aligned substrate on this differentiation. Furthermore, the ECM was analyzed for the presence, morphology, and gene expression of certain key ECM components. Finding the optimal cell seeding density is important since it is described by Harris et al that the cells density should be determined empirically for each cell type (44). Furthermore, Concaro et al., has shown that cell density influences collagen content produced by cells (45).

The optimization therefore allowed the production of a scaffold with the most favorable ECM. Alignment of ECM fibers were achieved in the aligned group, which is also supported by other studies by Bourget et al and Rubi-Sans et al, where both cells and ECM tend to align with the underlying substrate and therefore hold a potential for muscle regeneration (46,47). This cell migration and alignment occurs as a response to environmental cues such as substrate topography, called contact guidance, allowing the cells to move in accordance with the underlying surface and guide the cells through interaction with their cytoplasmic filopodia and focal adhesions (48–51).

The qualitative and quantitative assessment of collagenous components showed a noticeable decrease in both test groups when compared to the controls, which was further supported by the significant decrease in collagenous components reported by the quantitative analysis. There could be several explanations on why the deposition of ECM was reduced on the nanofibrous scaffolds. It is known that Polycaprolactone (PCL) is a hydrophobic material, and to enhance its surface properties and make it suitable for ECM attachment a fiber coating is needed (52). Therefore, polydopamine coating protocol was used to functionalize the fibers since it has a proved effect on the adhesion to PCL (53). In literature there is a degree of variability when it comes to concentration and incubation time of the polydopamine, which could affect the strength of ECM adhesion (53,54). Extensive evaluation of different substrate treatments on ECM deposition and attachment could not be conducted. This, in turn, could have resulted in a sub-optimal ECM adhesion in the test groups, and therefore could explain the reduced ECM presence. It can be hypothesized that different pre-treatment protocols such as plasma coating used by Miroshnichenko et al. or different coating molecule such as polynorepinephrine as described by Y. Liu et al., could result in a different ECM attachment environment. However these methods require more complex procedures (52,55).

In regard to ECM gene expression, it can be said that most target genes were either significantly downregulated at both timepoints or not significantly different from control at day 3. This is contrary to some data in the literature, such as the work from Bhattacharjee and colleagues which described that substrate alignment causes a significant increase in the expression of collagen I and decorin (56). However, in their study the smallest groove size analyzed was 5 µm with 5 µm wide plateau, whereas our scaffolds fibers were approximately 0.7 µm wide with an unknown fiber density (57), which could influence cell behavior. Furthermore, their qPCR procedure was conducted much later than in our study, namely after 21 days, which could allow the cells much longer time to adapt to their environment compared to just after 3 days from seeding. The difference in the cell type could also play a role in the gene expression, as corneal stem cells are situated in a highly aligned environment compared to hASC's and could therefore benefit more from the aligned substrate (58,59). For fibronectin and collagen VI, even though the initial expression was significantly reduced. At day 3 there was no statistically significant difference between both test groups and control. For fibronectin, this is supported by previous research by Almonacid et al., where ECM synthesized by human primary myoblasts showed no significant difference in fibronectin expression between a flat and an aligned substrate (60). However, given the different cell type it might not truly indicative as the protein deposition of e.g., fibronectin expression is generally lower compared to the hASCs (60). For collagen VI it was not possible compare our results to other research since the effect of alignment on collagen VI gene expression has so far not been elucidated in literature and we will here rely on the indirect immunofluorescent staining to determine its presence and discuss the findings. In literature, collagen VI has been shown to be not only a crucial component of the stem cell niche but also is central in satellite cell maintenance and muscle regeneration (32). Additionally, transplantation of collagen VI producing MSC in dystrophic mice showed improved muscle regeneration (61). Therefore, evidence suggests that collagen VI could be a vital yet overlooked component when assessing scaffolds for skeletal muscle regeneration.

For the Assessment of protein expression, it is indicative that the presence of all targeted ECM components was lower in the test groups compared to the control. However, an alignment of all targeted molecules was confirmed, which is also supported previously in the collagenous staining. This is in line with the findings of Wu et al., where the immunofluorescence imaging showed that both the ECM derived from corneal stroma cells and its subcomponents, like collagen I and VI, were confirmed to align themselves parallel with the underlying substrate (62). Even if there was a different cell type used compared to our study, it is assumed that ECM to substrate alignment is universal, as described by Rubi-Sans et al., and does not depend on cell type (46). This finding seems to suggest our scaffolds potential for skeletal muscle regeneration as substrate alignment is reported by Chen et al. and Zhao et al. amongst others to have increased muscle differentiation (63,64).

While myotube alignment was found in the aligned group, the ability of the ECM deposited on the scaffolds to promote muscle differentiation appears to be reduced in both test groups. Some of these results are at odds with literature, as reported by Smoak et al., where the aligned electrospun ECM scaffold significantly improved muscle differentiation and supported myotube alignment (65). The lower presence of myotubes could be explained by the significantly lower amount of ECM in the test groups. Still the ECM might influence muscle differentiation since the group without ECM contained slightly fewer myotubes than the ECM control group, possibly indicating a small positive effect on differentiation. This could indicate that hASC derived ECM is perhaps not the optimal substrate for differentiation of C2C12 myoblasts. Signs of unusual myoblast behavior were observed as early as 24 hours after seeding i.e., before differentiation on the ECM, where the cells became visibly elongated (appendix fig. 1), and growth appeared to be reduced in contrast to their normal slightly oval phenotype. Furthermore, the C2C12 appeared to exhibit some sort of ECM degradation mechanism, where the cells kept detaching the ECM after some time, causing an interruption of the experiment (appendix fig. 2). Our pilot study indicated a different cell behavior in regard to their interactions with ECM. The differences between the two groups could be explained by the difference in the cell behavior between the C2C12 cells and hSKMMs. As discussed by Langelaan et al., there were some proposed differences between the C2C12 and muscle progenitor cells which includes the hSKMMs. Indeed, the C2C12 is a long-lasting cell line while the hSKMMs are primary cells, designated for skeletal muscle regeneration. Genetic differences can result in a better more rapid maturation of hSKMMs myotubes (66). This could be a vital point to explore in further studies.

### 4.1 Limitations and Considerations

The timeframe for this project was limited, and due to the relative novelty of the experimental setup there were a lot of time-consuming challenges before proper data acquisition was possible, which influenced the scope of the projects. Furthermore, logistical challenges due to the COVID 19 pandemic drastically increased delivery times for certain key items. In particular, the extended acquisition time of the aligned and random well plates which were used in most of our experiments, caused substantial delays and thereby an exclusion of a planned glucose amino glycan assay and qPCR procedure for muscle differentiation which could have provided additional insights. We strongly recommend continuing to investigate the differential capacity of hSKMMs on ECM, as our pilot study shows potentially positive results.

## 5 Conclusions

In this study the effect of ECM orientation on skeletal muscle differentiation was assessed. While ECM fiber alignment was achieved, the expression of ECM components in the test groups was significantly lower than the control. A statistically significant reduction in expression of ECM genes was apparent at day 1 in both test groups, which persisted at day three for the expression of collagen I and decorin. Muscle differentiation was reduced in both test groups, with visually thinner and shorter myotubes, that like the ECM aligned themselves to the substrate's topography. The pilot examination of hSKMMs differentiation on ECM showed some promising results that could warrant further investigation on the ECM's effect on skeletal muscle differentiation. Therefore, we cannot accept our hypothesis that anisotropic ECM scaffolds have a positive effect on muscle differentiation due to their influence on cell alignment and maturation. To further clarify this hypothesis, more studies are needed to study the potential of aligned ECM for skeletal muscle regeneration.

# 7 Appendix

## Figure 1

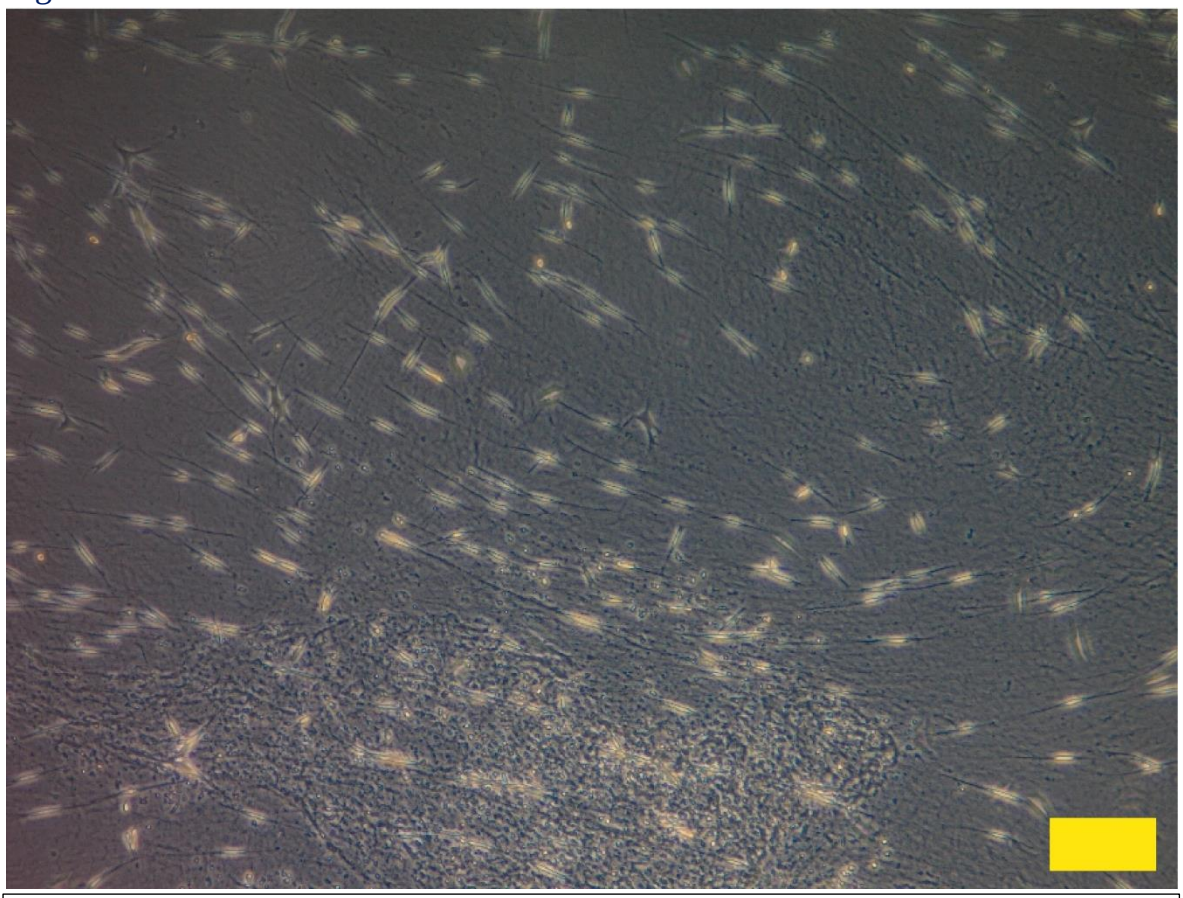

*Fig. 1. Illustration of the unusually elongated C2C12 cells on ECM control. Captured 24 hours after seeding. 40x magnification. Bar 200µm*

Figure 2

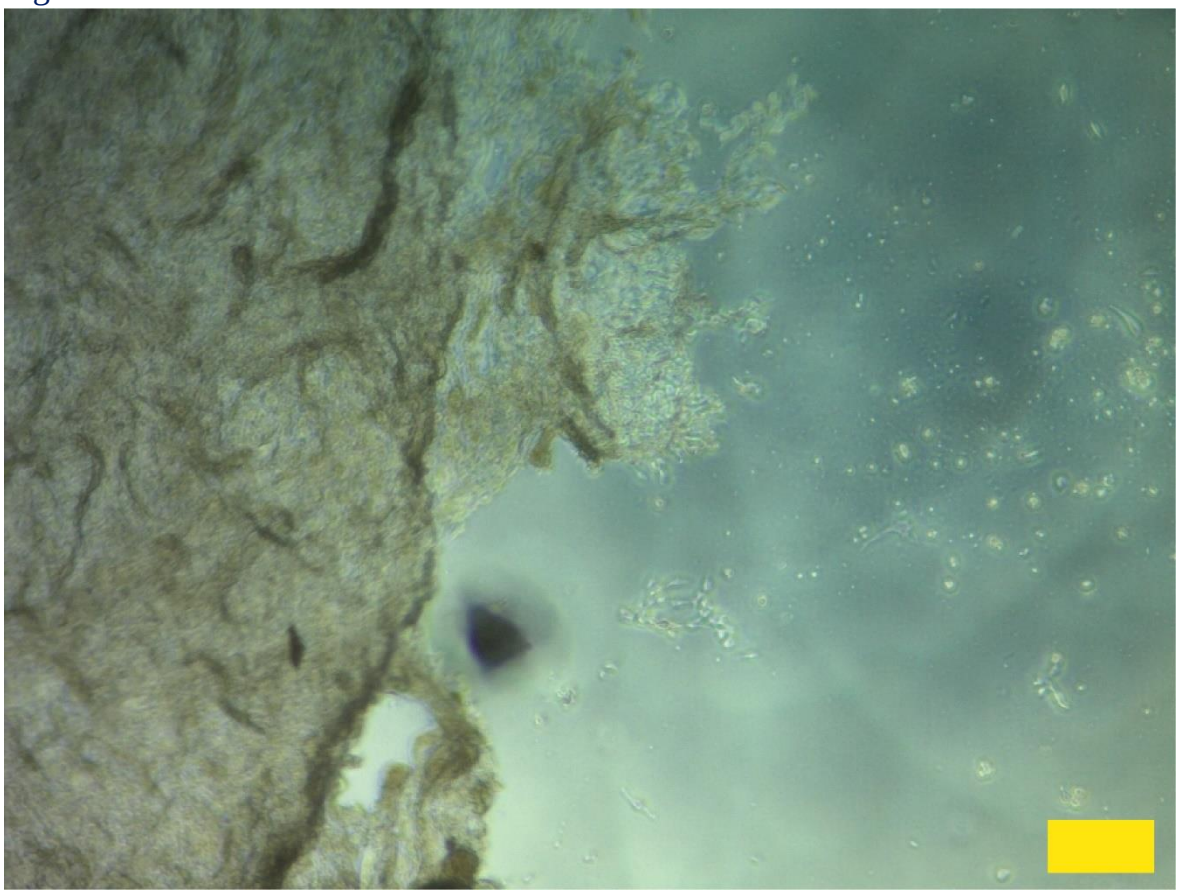

*Fig. 2. Illustration of ECM detachment influenced by C2C12 cells. 40x magnification. Bar 200µm*

# 6. Literature


1. Warren GL, Hulderman T, Jensen N, McKinstry M, Mishra M, Luster MI, et al. Physiological role of tumor necrosis factor α in traumatic muscle injury. The FASEB Journal [Internet]. 2002 Oct 1 [cited 2021 Aug 19];16(12):1630–2. Available from: https://faseb.onlinelibrary.wiley.com/doi/full/10.1096/fj.02-0187fje

2. Huard J, Lu A, Mu X, Guo P, Li Y. Muscle Injuries and Repair: What's New on the Horizon! Cells Tissues Organs [Internet]. 2016;202(3–4):227–36. Available from: https://www.karger.com/Article/FullText/443926

3. Liu J, Saul D, Böker KO, Ernst J, Lehman W, Schilling AF. Current Methods for Skeletal Muscle Tissue Repair and Regeneration. BioMed Research International. 2018;2018.

4. Kim JH, Kim I, Seol YJ, Ko IK, Yoo JJ, Atala A, et al. Neural cell integration into 3D bioprinted skeletal muscle constructs accelerates restoration of muscle function. Nature Communications 2020 11:1 [Internet]. 2020 Feb 24 [cited 2021 Jul 14];11(1):1–12. Available from: https://www.nature.com/articles/s41467-020-14930-9

5. Järvinen TAH, Järvinen TLN, Kääriäinen M, Kalimo H, Järvinen M. Muscle injuries: Biology and treatment [Internet]. Vol. 33, American Journal of Sports Medicine. SAGE PublicationsSage CA: Los Angeles, CA; 2005 [cited 2021 Jun 26]. p. 745–64. Available from: https://journals-sagepub-com.zorac.aub.aau.dk/doi/full/10.1177/0363546505274714

6. Quintero AJ, Wright VJ, Fu FH, Huard J. Stem Cells for the Treatment of Skeletal Muscle Injury [Internet]. Vol. 28, Clinics in Sports Medicine. NIH Public Access; 2009 [cited 2021 Jun 26]. p. 1–11. Available from: /pmc/articles/PMC2630112/

7. Höke A, Brushart T. Introduction to special issue: Challenges and opportunities for regeneration in the peripheral nervous system. Vol. 223, Experimental Neurology. Academic Press; 2010. p. 1–4.

8. Liao H, Zhou GQ. Development and Progress of Engineering of Skeletal Muscle Tissue. Tissue Engineering Part B: Reviews [Internet]. 2009 Sep 1 [cited 2021 Jul 25];15(3):319–31. Available from: https://www.liebertpub.com/doi/10.1089/ten.teb.2009.0092

9. Kim JH, Seol YJ, Ko IK, Kang HW, Lee YK, Yoo JJ, et al. 3D Bioprinted Human Skeletal Muscle Constructs for Muscle Function Restoration. Scientific Reports [Internet]. 2018 Dec 1 [cited 2021 Jun 30];8(1):12307. Available from: www.nature.com/scientificreports

10. Pratesi A, Tarantini F, Bari M di. Skeletal muscle: an endocrine organ. Clinical Cases in Mineral and Bone Metabolism [Internet]. 2013 [cited 2021 Jul 27];10(1):11. Available from: /pmc/articles/PMC3710002/

11. Gholobova D, Terrie L, Gerard M, Declercq H, Thorrez L. Vascularization of tissue-engineered skeletal muscle constructs. Vol. 235, Biomaterials. Elsevier Ltd; 2020. p. 119708.

12. Frontera WR, Ochala J. Skeletal Muscle: A Brief Review of Structure and Function [Internet]. Vol. 45, Behavior Genetics. Springer New York LLC; 2015 [cited 2021 Jun 25]. p. 183–95. Available from: https://link.springer.com/article/10.1007/s00223-014-9915-y

13. Lieber RL, Fridén J. Clinical Significance of Skeletal Muscle Architecture. Clinical Orthopaedics and Related Research [Internet]. 2001 Feb;383:140–51. Available from: http://journals.lww.com/00003086-200102000-00016

14. Gotti C, Sensini A, Fornaia G, Gualandi C, Zucchelli A, Focarete ML. Biomimetic Hierarchically Arranged Nanofibrous Structures Resembling the Architecture and the Passive Mechanical Properties of Skeletal Muscles: A Step Forward Toward Artificial Muscle. Frontiers in Bioengineering and Biotechnology [Internet]. 2020 Jul 16 [cited 2021 Jun 30];8:767. Available from: www.frontiersin.org

15. Urciuolo A, Urbani L, Perin S, Maghsoudlou P, Scottoni F, Gjinovci A, et al. Decellularised skeletal muscles allow functional muscle regeneration by promoting host cell migration. Scientific Reports 2018 8:1 [Internet]. 2018 May 30 [cited 2021 Oct 10];8(1):1–20. Available from: https://www.nature.com/articles/s41598-018-26371-y

16. Porzionato A, Sfriso MM, Pontini A, Macchi V, Petrelli L, Pavan PG, et al. Decellularized Human Skeletal Muscle as Biologic Scaffold for Reconstructive Surgery. International Journal of Molecular Sciences 2015, Vol 16, Pages 14808-14831 [Internet]. 2015 Jul 1 [cited 2021 Oct 10];16(7):14808–31. Available from: https://www.mdpi.com/1422-0067/16/7/14808/htm

17. Garreta E, Oria R, Tarantino C, Pla-Roca M, Prado P, Fernández-Avilés F, et al. Tissue engineering by decellularization and 3D bioprinting. Materials Today. 2017 May 1;20(4):166–78.

18. Riis S, Hansen AC, Johansen L, Lund K, Pedersen C, Pitsa A, et al. Fabrication and characterization of extracellular matrix scaffolds obtained from adipose-derived stem cells. Methods. 2020 Jan 15;171:68–76.

19. Charvet B, Ruggiero F, le Guellec D. The development of the myotendinous junction. A review. Vol. 2, Ligaments and Tendons Journal. 2012.

20. Fernandes TL, Pedrinelli A, Hernandez AJ. MUSCLE INJURY – PHYSIOPATHOLOGY, DIAGNOSIS, TREATMENT AND CLINICAL PRESENTATION. Revista Brasileira de Ortopedia (English Edition). 2011 May;46(3):247–55.

21. Patel KH, Dunn AJ, Talovic M, Haas GJ, Marcinczyk M, Elmashhady H, et al. Aligned nanofibers of decellularized muscle ECM support myogenic activity in primary satellite cells in vitro. Biomedical Materials [Internet]. 2019 Apr 3 [cited 2022 May 18];14(3):035010. Available from: https://iopscience-iop-org.zorac.aub.aau.dk/article/10.1088/1748-605X/ab0b06

22. Corona BT, Rivera JC, Owens JG, Wenke JC, Rathbone CR. Volumetric muscle loss leads to permanent disability following extremity trauma. Journal of Rehabilitation Research and Development. 2015;52(7):785–92.

23. Grounds MD. Complexity of Extracellular Matrix and Skeletal Muscle Regeneration. In: Skeletal Muscle Repair and Regeneration [Internet]. Dordrecht: Springer Netherlands; 2008. p. 269–302. Available from: http://link.springer.com/10.1007/978-1-4020-6768-6_13

24. Tsuchiya Y, Kitajima Y, Masumoto H, Ono Y. Damaged Myofiber-Derived Metabolic Enzymes Act as Activators of Muscle Satellite Cells. Stem Cell Reports. 2020 Oct 13;15(4):926–40.

25. Kurosaka M, Machida S. Interleukin-6-induced satellite cell proliferation is regulated by induction of the JAK2/STAT3 signalling pathway through cyclin D1 targeting. Cell Proliferation [Internet]. 2013 Aug [cited 2021 Nov 10];46(4):365. Available from: /pmc/articles/PMC6496007/

26. Frantz C, Stewart KM, Weaver VM. The extracellular matrix at a glance. Journal of Cell Science [Internet]. 2010 Dec 15 [cited 2022 Jan 4];123(24):4195. Available from: /pmc/articles/PMC2995612/

27. Kang MS, Lee SH, Park WJ, Lee JE, Kim B, Han DW. Advanced techniques for skeletal muscle tissue engineering and regeneration. Bioengineering. 2020 Sep 1;7(3):1–14.

28. Gilbert-Honick J, Ginn B, Zhang Y, Salehi S, Wagner KR, Mao HQ, et al. Adipose-derived Stem/Stromal Cells on Electrospun Fibrin Microfiber Bundles Enable Moderate Muscle Reconstruction in a Volumetric Muscle Loss Model. Cell Transplantation [Internet]. 2018 Nov 1 [cited 2022 May 18];27(11):1644–56. Available from: https://journals.sagepub.com/doi/10.1177/0963689718805370

29. Zhang W, Liu Y, Zhang H. Extracellular matrix: an important regulator of cell functions and skeletal muscle development. Cell & Bioscience 2021 11:1 [Internet]. 2021 Mar 31 [cited 2021 Dec 7];11(1):1–13. Available from: https://cellandbioscience.biomedcentral.com/articles/10.1186/s13578-021-00579-4

30. Kular JK, Basu S, Sharma RI. The extracellular matrix: Structure, composition, age-related differences, tools for analysis and applications for tissue engineering. Journal of Tissue Engineering [Internet]. 2014 Jan 17 [cited 2022 Apr 19];5. Available from: /pmc/articles/PMC4883592/

31. Liu X, Gao Y, Long X, Hayashi T, Mizuno K, Hattori S, et al. Type I collagen promotes the migration and myogenic differentiation of C2C12 myoblasts via the release of interleukin-6 mediated by FAK/NF-κB p65 activation. Food Funct [Internet]. 2020 Jan 1 [cited 2022 Apr 19];11(1):328–38. Available from: https://pubmed.ncbi.nlm.nih.gov/31799535/

32. Urciuolo A, Quarta M, Morbidoni V, Gattazzo F, Molon S, Grumati P, et al. Collagen VI regulates satellite cell self-renewal and muscle regeneration. Nature Communications 2013 4:1 [Internet]. 2013 Jun 7 [cited 2021 Dec 9];4(1):1–13. Available from: https://www.nature.com/articles/ncomms2964

33. Vaz R, Martins GG, Thorsteinsdóttir S, Rodrigues G. Fibronectin promotes migration, alignment and fusion in an in vitro myoblast cell model. Cell and Tissue Research [Internet]. 2012 Jun 18 [cited 2022 Apr 19];348(3):569–78. Available from: https://link-springer-com.zorac.aub.aau.dk/article/10.1007/s00441-012-1364-1

34. Li Y, Li J, Zhu J, Sun B, Branca M, Tang Y, et al. Decorin Gene Transfer Promotes Muscle Cell Differentiation and Muscle Regeneration. Molecular Therapy. 2007 Sep 1;15(9):1616–22.

35. Kuraitis D, Berardinelli MG, Suuronen EJ, Musarò A. A necrotic stimulus is required to maximize matrix-mediated myogenesis in mice. DMM Disease Models and Mechanisms [Internet]. 2013 May 1 [cited 2022 Mar 10];6(3):793–801. Available from: https://journals.biologists.com/dmm/article/6/3/793/3408/A-necrotic-stimulus-is-required-to-maximize-matrix

36. Tsuji W, Rubin JP, Marra KG. Adipose-derived stem cells: Implications in tissue regeneration. World Journal of Stem Cells [Internet]. 2014 [cited 2022 Mar 8];6(3):312. Available from: /pmc/articles/PMC4131273/

37. Hassanshahi A, Hassanshahi M, Khabbazi S, Hosseini-Khah Z, Peymanfar Y, Ghalamkari S, et al. Adipose-derived stem cells for wound healing. J Cell Physiol [Internet]. 2019 Jun 1 [cited 2022 Mar 8];234(6):7903–14. Available from: https://pubmed.ncbi.nlm.nih.gov/30515810/

38. Alexeev V, Arita M, Donahue A, Bonaldo P, Chu ML, Igoucheva O. Human adipose-derived stem cell transplantation as a potential therapy for collagen VI-related congenital muscular dystrophy. Stem Cell Research and Therapy [Internet]. 2014 Feb 12 [cited 2022 May 18];5(1):1–17. Available from: https://link.springer.com/articles/10.1186/scrt411

39. Hyldig K, Riis S, Pennisi CP, Zachar V, Fink T. Implications of Extracellular Matrix Production by Adipose Tissue-Derived Stem Cells for Development of Wound Healing Therapies. International Journal of Molecular Sciences [Internet]. 2017 Jun 1 [cited 2022 May 18];18(6). Available from: /pmc/articles/PMC5485991/

40. Azam Bozorgi Zarrini, Bozorgi M, Khazaei M, Soleimani M. Decellularized Extracellular Matrices in Bone Tissue Engineering: From Cells to Tissues. Mini-Review. Cell and Tissue Biology [Internet]. 2020 Nov 1 [cited 2022 May 18];14(6):399–406. Available from: https://link-springer-com.zorac.aub.aau.dk/article/10.1134/S1990519X20060127

41. Hussey GS, Dziki JL, Badylak SF. Extracellular matrix-based materials for regenerative medicine. Nature Reviews Materials 2018 3:7 [Internet]. 2018 May 29 [cited 2022 May 18];3(7):159–73. Available from: https://www.nature.com/articles/s41578-018-0023-x

42. Kuznetsova IM, Turoverov KK, Uversky VN. What Macromolecular Crowding Can Do to a Protein. International Journal of Molecular Sciences 2014, Vol 15, Pages 23090-23140 [Internet]. 2014 Dec 12 [cited 2022 May 9];15(12):23090–140. Available from: https://www.mdpi.com/1422-0067/15/12/23090/htm

43. Kulp DT, Herzfeld J. Crowding-induced organization of cytoskeletal elements. III. Spontaneous bundling and sorting of self-assembled filaments with different flexibilities. Biophysical Chemistry. 1995 Dec 1;57(1):93–102.

44. Harris GM, Raitman I, Schwarzbauer JE. Cell-derived decellularized extracellular matrices. Methods Cell Biol [Internet]. 2018 [cited 2022 May 25];143:97. Available from: /pmc/articles/PMC5995326/

45. Concaro S, Nicklasson E, Ellowsson L, Lindahl A, Brittberg M, Gatenholm P. Effect of cell seeding concentration on the quality of tissue engineered constructs loaded with adult human articular chondrocytes. Journal of Tissue Engineering and Regenerative Medicine. 2008 Jan;2(1):14–21.

46. Rubi-Sans G, Castaño O, Cano I, Mateos-Timoneda MA, Perez-Amodio S, Engel E. Engineering Cell-Derived Matrices: From 3D Models to Advanced Personalized Therapies. Advanced Functional Materials [Internet]. 2020 Oct 1 [cited 2022 May 15];30(44):2000496. Available from: https://onlinelibrary.wiley.com/doi/full/10.1002/adfm.202000496

47. Bourget JM, Guillemette M, Veres T, Auger FA, Germain L. Alignment of Cells and Extracellular Matrix Within Tissue- Engineered Substitutes. Advances in Biomaterials Science and Biomedical Applications [Internet]. 2013 Mar 27 [cited 2022 May 15]; Available from: https://www.intechopen.com/chapters/43740

48. Provenzano PP, Inman DR, Eliceiri KW, Trier SM, Keely PJ. Contact Guidance Mediated Three-Dimensional Cell Migration is Regulated by Rho/ROCK-Dependent Matrix Reorganization. Biophysical Journal. 2008 Dec 1;95(11):5374–84.

49. Ramirez-San Juan GR, Oakes PW, Gardel ML. Contact guidance requires spatial control of leading-edge protrusion. Molecular Biology of the Cell [Internet]. 2017 Apr 4 [cited 2022 May 23];28(8):1043. Available from: /pmc/articles/PMC5391181/

50. Londono C, Loureiro MJ, Slater B, Lücker PB, Soleas J, Sathananthan S, et al. Nonautonomous contact guidance signaling during collective cell migration. Proc Natl Acad Sci U S A [Internet]. 2014 Feb 4 [cited 2022 May 23];111(5):1807–12. Available from: www.pnas.org/cgi/doi/10.1073/pnas.1321852111

51. Andersen JI, Pennisi CP, Fink T, Zachar V. Focal Adhesion Kinase Activation Is Necessary for Stretch-Induced Alignment and Enhanced Differentiation of Myogenic Precursor Cells. Tissue Engineering - Part A [Internet]. 2018 Apr 1 [cited 2022 May 24];24(7–8):631–40. Available from: https://www-liebertpub-com.zorac.aub.aau.dk/doi/full/10.1089/ten.tea.2017.0137

52. Miroshnichenko S, Timofeeva V, Permykova E, Ershov S, Kiryukhantsev-Korneev P, Dvořaková E, et al. Plasma-Coated Polycaprolactone Nanofibers with Covalently Bonded Platelet-Rich Plasma Enhance Adhesion and Growth of Human Fibroblasts. Nanomaterials [Internet]. 2019 Apr 1 [cited 2022 May 15];9(4):637. Available from: /pmc/articles/PMC6523319/

53. Zuppolini S, Cruz-Maya I, Guarino V, Borriello A. Optimization of Polydopamine Coatings onto Poly–ε–Caprolactone Electrospun Fibers for the Fabrication of Bio-Electroconductive Interfaces. Journal of Functional Biomaterials 2020, Vol 11, Page 19 [Internet]. 2020 Mar 17 [cited 2022 May 15];11(1):19. Available from: https://www.mdpi.com/2079-4983/11/1/19/htm

54. Murari G, Bock N, Zhou H, Yang L, Liew T, Fox K, et al. Effects of polydopamine coatings on nucleation modes of surface mineralization from simulated body fluid. Scientific Reports

2020 10:1 [Internet]. 2020 Sep 11 [cited 2022 May 15];10(1):1–9. Available from: https://www.nature.com/articles/s41598-020-71900-3

55. Liu Y, Zhou G, Liu Z, Guo M, Jiang X, Taskin MB, et al. Mussel Inspired Polynorepinephrine Functionalized Electrospun Polycaprolactone Microfibers for Muscle Regeneration. Scientific Reports 2017 7:1 [Internet]. 2017 Aug 15 [cited 2022 May 15];7(1):1–10. Available from: https://www.nature.com/articles/s41598-017-08572-z

56. Bhattacharjee P, Cavanagh BL, Ahearne M. Effect of substrate topography on the regulation of human corneal stromal cells. Colloids and Surfaces B: Biointerfaces. 2020 Jun 1;190:110971.

57. Nanofiber Solutions. Nanofiber Plates - Nanofiber Solutions [Internet]. 2022 [cited 2022 May 16]. Available from: https://nanofibersolutions.com/product/nanofiber-plates/

58. Blackburn BJ, Jenkins MW, Rollins AM, Dupps WJ. A review of structural and biomechanical changes in the cornea in aging, disease, and photochemical crosslinking. Frontiers in Bioengineering and Biotechnology. 2019;7(MAR):66.

59. Eto H, Suga H, Matsumoto D, Inoue K, Aoi N, Kato H, et al. Characterization of structure and cellular components of aspirated and excised adipose tissue. Plastic and Reconstructive Surgery. 2009 Oct;124(4):1087–97.

60. Almonacid Suarez AM, Brinker MGL, Brouwer LA, van der Ham I, Harmsen MC, van Rijn P. Topography-Mediated Myotube and Endothelial Alignment, Differentiation, and Extracellular Matrix Organization for Skeletal Muscle Engineering. Polymers (Basel). 2020 Aug 28;12(9):1948.

61. Takenaka-Ninagawa N, Kim J, Zhao M, Sato M, Jonouchi T, Goto M, et al. Collagen-VI supplementation by cell transplantation improves muscle regeneration in Ullrich congenital muscular dystrophy model mice. Stem Cell Research and Therapy [Internet]. 2021 Dec 1 [cited 2022 May 24];12(1):1–18. Available from: https://stemcellres.biomedcentral.com/articles/10.1186/s13287-021-02514-3

62. Wu J, Du Y, Watkins SC, Funderburgh JL, Wagner WR. The engineering of organized human corneal tissue through the spatial guidance of corneal stromal stem cells. Biomaterials. 2012 Feb 1;33(5):1343–52.

63. Chen MC, Sun YC, Chen YH. Electrically conductive nanofibers with highly oriented structures and their potential application in skeletal muscle tissue engineering. Acta Biomaterialia. 2013 Mar 1;9(3):5562–72.

64. Zhao Y, Zeng H, Nam J, Agarwal S. Fabrication of skeletal muscle constructs by topographic activation of cell alignment. Biotechnology and Bioengineering [Internet]. 2009 Feb 1 [cited 2022 May 23];102(2):624–31. Available from: https://onlinelibrary-wiley-com.zorac.aub.aau.dk/doi/full/10.1002/bit.22080

65. Smoak MM, Hogan KJ, Grande-Allen KJ, Mikos AG. Bioinspired electrospun dECM scaffolds guide cell growth and control the formation of myotubes. Sci Adv [Internet]. 2021 [cited 2021 Jul 20];7:4123–37. Available from: http://advances.sciencemag.org/

66. Langelaan MLP, Boonen KJM, Rosaria-Chak KY, van der Schaft DWJ, Post MJ, Baaijens FPT. Advanced maturation by electrical stimulation: Differences in response between C2C12 and primary muscle progenitor cells. Journal of Tissue Engineering and Regenerative Medicine [Internet]. 2011 Jul 1 [cited 2022 May 22];5(7):529–39. Available from: https://onlinelibrary-wiley-com.zorac.aub.aau.dk/doi/full/10.1002/term.345

67. Biga LM, Dawson S, Harwell A, Hopkins R, Kaufmann J, LeMaster M, et al. Illustration of selected anatomical structures in skeletal muscels. Anatomy & Physiology . OpenStax; 2022.

68. Schmidt M, Schüler SC, Hüttner SS, von Eyss B, von Maltzahn J. Adult stem cells at work: regenerating skeletal muscle. Cellular and Molecular Life Sciences. 2019 Jul 15;76(13):2559–70.